Fearless Luminance Adaptation: A Macro-Micro-Hierarchical Transformer for Exposure Correction

Gehui Li

Dalian University of Technology gehuili90@gmail.com

Zhiying Jiang Dalian University of Technology zyjiang0630@gmail.com Jinyuan Liu Dalian University of Technology atlantis918@hotmail.com

Xin Fan
Dalian University of Technology
xin.fan@dlut.du.cn

Long Ma
Dalian University of Technology
malone94319@gmail.com

Risheng Liu*
Dalian University of Technology
Peng Cheng Laboratory
rsliu@dlut.edu.cn



Figure 1: The row displays a visual comparison of two cutting-edge methods alongside our proposed one, implemented on five separate exposures (ranging from +1.5EV to -1.5EV). It is crucial to emphasize that our method not only precisely corrects color distortions but also ensures consistency of the correction results.

ABSTRACT

Photographs taken with less-than-ideal exposure settings often display poor visual quality. Since the correction procedures vary significantly, it is difficult for a single neural network to handle all exposure problems. Moreover, the inherent limitations of convolutions, hinder the models ability to restore faithful color or details on extremely over-/under- exposed regions. To overcome these limitations, we propose a Macro-Micro-Hierarchical transformer, which consists of a macro attention to capture long-range dependencies, a micro attention to extract local features, and a hierarchical structure for coarse-to-fine correction. In specific, the complementary macro-micro attention designs enhance locality while allowing global interactions. The hierarchical structure enables the network to correct exposure errors of different scales layer by layer. Furthermore, we propose a contrast constraint and couple it seamlessly in the loss function, where the corrected image is pulled towards the positive sample and pushed away from the dynamically generated negative samples. Thus the remaining color distortion and loss of detail can be removed. We also extend our method as an image

enhancer for low-light face recognition and low-light semantic

CCS CONCEPTS

• Computing methodologies → Computational photography.

KEYWORDS

Image restoration, Exposure correction, Low-light enhancement, Low-light semantic segmentation, Low-light face detection

ACM Reference Format:

Gehui Li, Jinyuan Liu, Long Ma, Zhiying Jiang, Xin Fan, and Risheng Liu. 2023. Fearless Luminance Adaptation: A Macro-Micro-Hierarchical Transformer for Exposure Correction. In *Proceedings of the 31st ACM International Conference on Multimedia (MM '23), October 29–November 3, 2023, Ottawa, ON, Canada.* ACM, New York, NY, USA, 10 pages. https://doi.org/10.1145/3581783.3612436

1 INTRODUCTION

The ever-increasing interest in photography has intensified the need to capture expansive scenes under diverse lighting conditions. Nevertheless, image color and detail can be significantly compromised by sub-optimal and non-uniform illumination. While professional photographers often tackle exposure issues with specialized equipment and software, these solutions necessitate considerable expertise and can be costly. Moreover, harsh exposure conditions can adversely impact the performance of downstream computer vision tasks. Consequently, there is a pressing need for a model

Permission to make digital or hard copies of all or part of this work for personal or classroom use is granted without fee provided that copies are not made or distributed for profit or commercial advantage and that copies bear this notice and the full citation on the first page. Copyrights for components of this work owned by others than the author(s) must be honored. Abstracting with credit is permitted. To copy otherwise, or republish, to post on servers or to redistribute to lists, requires prior specific permission and/or a fee. Request permissions from permissions@acm.org.

MM '23, October 29-November 3, 2023, Ottawa, ON, Canada.

© 2023 Copyright held by the owner/author(s). Publication rights licensed to ACM. ACM ISBN 979-8-4007-0108-5/23/10...\$15.00 https://doi.org/10.1145/3581783.3612436

segmentation. Experiments demonstrate that our approach obtains more attractive results than state-of-the-art methods quantitatively and qualitatively.

 $^{^{\}star}$ Corresponding author: Risheng Liu.

capable of correcting images with a wide range of exposure errors to achieve consistent, normal exposure without sacrificing color fidelity or detail.

Existing models [13, 22, 36, 39, 40, 43–45, 53, 56] primarily addressing single exposure error scenarios perform inadequately when confronted with images containing multiple exposure errors. Predicated on the assumption that scene lighting is low-light, these methods are inherently ill-equipped to adapt to varying exposure states. In addition, multi-exposure fusion methods [30, 31, 33, 34, 38] are powerless when there is only one image of the same scene. These limitation have spurred the development of new approaches [1, 7, 11, 45, 52] for tackling multiple exposure errors.

MSEC[1] addresses exposure correction of input images under diverse lighting. LCDP[52] is designed to tackle the challenge of multiple exposure errors within a single image. However, existing approaches suffer from two critical shortcomings. First, when presented with a set of images with different exposure errors for the same scene, these methods fail to achieve a consistent correction state, leading to considerable discrepancies in the correction outcomes. Second, they struggle to restore distorted details in heavily overexposed and underexposed areas, resulting in unbalanced and lackluster colors in the corrected images.

Recognizing the importance of addressing the irreversible color distortion in severely overexposed or underexposed regions, we advocate for the utilization of richer semantic information from neighboring regions to compensate for the lost color. By providing the network with enhanced access to multi-scale information, the recovery of color-distorted regions is facilitated. To this end, we propose the Macro-Micro Transformer Restorer (MMT Restorer). Simultaneously, we introduce a dynamic negative sample generator and a contrast constraint function. By incorporating a substantial number of high-quality negative samples, the network learns a more consistent criterion, ultimately enhancing the consistency of input image correction. Furthermore, we present the Macro-Micro-Hierarchical Transformer (MMHT), a hierarchical extension of MMT Restorer, which refines the correction process from coarse to fine, further improving the quality of the corrected images.

The contributions of this paper are as follows:

- We propose a Macro-Micro-Hierarchical Transformer, which, in comparison to existing methods, yields visually appealing colors and consistently corrected outcomes.
- Considering the limited capacity of convolutions to attend to non-local regions, we design a Macro-Micro Attention mechanism that effectively restores distorted color by strengthening global dependencies.
- To explore the intrinsic information of over-/under- exposed image and the reference one, we raises a hierarchical contrastive learning scheme. In this manner, the restored image is pulled to the reference image and pushed away from the multiple exposed ones in a hierarchical latent feature spaces.
- Extensive experimental results demonstrate our method empirically realizes the remarkable promotion in color and consistency of corrected images, as well as standard accuracy for low-light segmentation and detection compared with existing advanced networks.

2 RELATED WORK

2.1 Methods against Harsh Lighting Condition

Low-Light Enhancement. Traditional methods[3, 12, 12, 14, 35, 37, 40, 58, 67, 69] based on Retinex theory have been favored in recent years. These methods mainly decompose the image into reflectance map and illumination map, and then do processing on them separately to get the final result. Therefore, the goal is to predict the illumination map to obtain a well-exposed target image. Some deep learning-based methods[6, 10, 18–21, 23, 28, 32, 53, 56, 65, 71] have also emerged subsequently. All these works are limited to image correction for underexposure conditions. However, mis-exposed images are common in reality, which also contain a large number of over-exposed and unevenly exposed images. Therefore, our goal is to construct a model capable of simultaneously correcting images with these different exposure levels.

Exposure Correction. MSEC[1] proposes a coarse-to-fine deep learning approach that focuses for the first time on the task of simultaneously correcting overexposed and underexposed images. IAT[7] decomposes the Image Signal Processor (ISP) into local and global image components to correct the image from low-light or overexposure conditions and proceeds to solve the problem of low-light image semantic segmentation. LCDP[52] proposes the LCDE module with Dual-Illumination mechanism to solve the problem of having multiple exposure errors on a single image. However, existing methods still have two common problems: inconsistent correction results and non-enjoyable colors. In this paper, we propose a Macro-Micro-Hierarchical Transformer to solve them.

2.2 Vision Transformers

A number of image restorers designed using transformer have appeared. For example, Uformer[55] replaces the building block with its proposed LeWin Transformer Block based on the Encoder-Decoder structure of U-Net, which consists of window attention with a sliding window[41] and Locally Enhanced Feed-forward[62]. Restormer [63] proposes Transformer Block consisting of A Multi-Dconv Head Transposed Attention with Gated Dconv Feed-forward Network. But these general image restorers, have a common problem that they do not adapt well to the exposure correction problem. In this paper, we propose a Macro-Micro Transformer Block containing two mechanisms of complementary Attention to solve this problem. Although Transformers has a stronger model fitting capability, it requires far more data than CNNs because of the lack of inductive bias. How to effectively combine the strengths of both is an important issue. A large number of networks [47, 48, 57, 62, 64, 66] designed for high level tasks in recent years have organically combined convolution and transformer. The Coatnet[9] is particularly enlightening in its exploration of the arrangement of convolution building blocks and transformer building blocks. Using a similar experimental method, we design the final network structure and its better adaptation to our task.

3 METHOD

3.1 The overall of the proposed method

Our proposed method commences with a Laplace decomposition to obtain four-layer decomposed images, L1-L4, derived from the

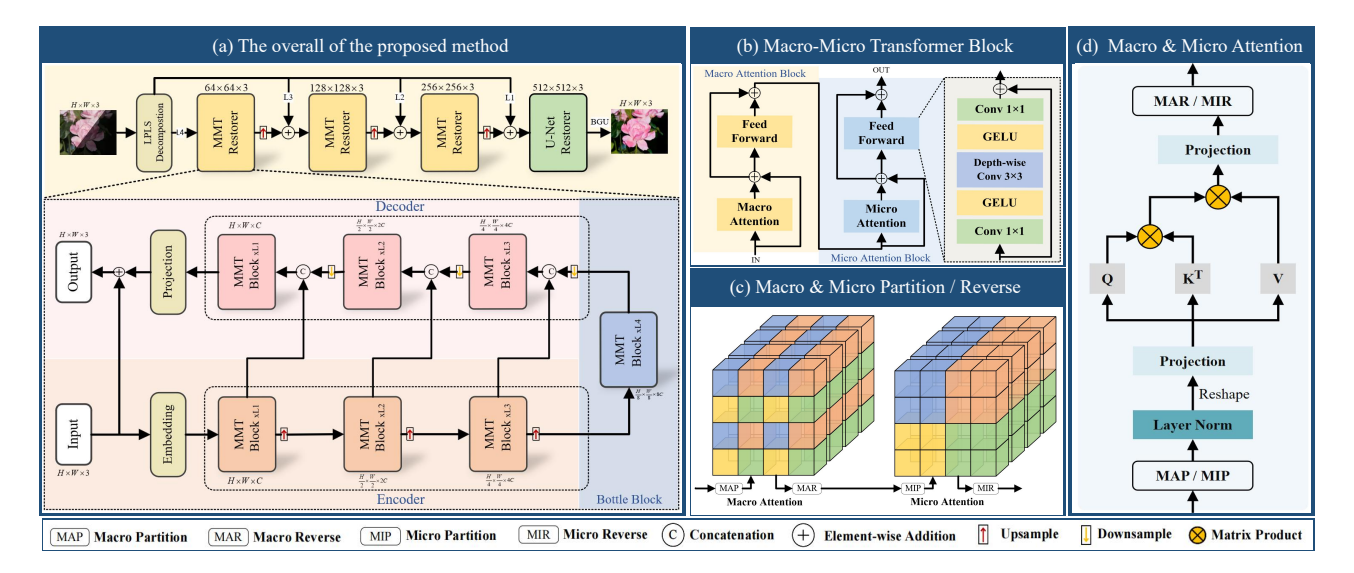


Figure 2: (a) The architecture of our MMHT method, which contains MMT Restorer and U-Net Restorer to reconstruct the normal exposure image. (b) Macro-Micro Transformer Block with two complementary attention mechanisms to capture global dependencies. (c) Diagram of Micro & Macro Attention Partition. (d) The structure of Micro & Macro Attention.

input image. These decomposed images serve as the input terms for the skip-connection. The primary objective of this operation is to decompose the source images into distinct spatial frequency bands, thereby enabling the utilization of separate networks for the restoration of colors and details in specific frequency bands at varying decomposition levels. The L4 image is fed into the network as the initial term. The architecture of the network comprises four stages, with stages 1, 2, and 3 designated for the Macro-Micro Transformer Restorer (MMT Restorer) and stage 4 for the U-Net Restorer. In the final stage, we employ a convolution-based structure as a substitute for the MMT Restorer. This decision is motivated by the fact that the transformer sacrifices its inductive bias while acquiring a global perceptual field through the attention structure. Consequently, we construct the U-Net Restorer by replacing the MMT Block with multi-layer convolutions, while preserving the overall structure of the MMT Restorer. In combination with convolution, our method achieves superior correction results. An additional benefit of this approach is that implementing convolution on larger sizes reduces the computation complexity. Following each stage, up-sampling is performed to double the width and height. Ultimately, the 512×512 size image is up-sampled by BGU[4] to its original size, yielding the final output. A schematic representation of the framework is depicted in Figure 2.

3.2 Macro-Micro Transformer Restorer

As illustrated in Figure 2 (a), the specific structure of our method is as follows. Given an input image, its dimensions are initially increased by an Embedding layer to C. Subsequently, the input is processed through an Encoder consisting of three stages, wherein identical MMT Blocks are stacked repeatedly with L_i layers in each stage. Upon generating the feature output, the image size is downsampled using pooling, and the dimensions are increased via point-wise convolution. Following feature extraction by the

Encoder, initial semantic features are obtained. These semantic features are further refined using the Bottle Block, which serves as input for the Decoder to guide the generation of exposure-corrected images. Prior to feeding the image into the subsequent stage, it is upsampled using Pixel-shuffle[51] and concatenated with the features processed by the Encoder at the same stage via a skip connection. In a similar way, the dimensionality is reduced to 3 by the Projection layer, and the resulting output is added to the input image to produce the exposure-corrected image.

3.3 Macro-Micro Transformer Block

In MMT Restorer, we alternately arrange Macro Attention and Micro Attention to obtain global and local features, but with linear complexity for spatial dimensions. Diagram is shown in Figure 2 (b). The formulas of spatial attention is as follows.

$$\mathcal{A}_{Spatial}(\mathbf{Q}, \mathbf{K}, \mathbf{V}) = Concat \left(head_1, \dots, head_{\frac{C}{H_d}} \right),$$
 (1)

where
$$\text{head}_i = \text{Softmax}\left(\frac{\mathbf{Q}_i \mathbf{K}_i^T}{\sqrt{H_d}}\right) \mathbf{V}_i$$
. $\mathbf{Q}_i = \mathbf{X}_i \mathbf{W}_i^Q$, $\mathbf{K}_i = \mathbf{X}_i \mathbf{W}_i^K$ and

 $\mathbf{V}_i = \mathbf{X}_i \mathbf{W}_i^V \in \mathbb{R}^{P \times H_d}$. \mathbf{W}_i denotes the projection weights of the i_{th} head for \mathbf{Q}_i , \mathbf{K}_i , \mathbf{V}_i . P is is the number of total patches. H_d is head dimension. C is the total channel size.

3.3.1 Micro Attention. Conventional transformers employ global attention computation, resulting in a quadratic computational complexity. In contrast, Micro Attention confines attention computation to each window, effectively reducing the computational burden. Micro Partition: $(\frac{H}{D}\times D,\frac{W}{D}\times D,C)\to (\frac{HW}{D^2},D^2,C).$ After partition, we have the following formula.

$$MSA_{Micro}(\mathbf{Q}, \mathbf{K}, \mathbf{V}) = \left\{ \mathcal{A}_{Spatial}(\mathbf{Q}_j, \mathbf{K}_j, \mathbf{V}_j) \right\}_{j=0}^{\frac{HW}{D^2}}, \quad (2)$$

where $\mathbf{Q}_j, \mathbf{K}_j, \mathbf{V}_j \in \mathbb{R}^{D^2 \times C}$ are local window queries, keys, and values. Each window contains $\mathbf{D} \times \mathbf{D}$ patches.

Despite this significant reduction in computation, the exclusive focus on the window attention results in the loss of global information modeling capabilities. To address this limitation, we propose Macro Attention, characterized by a larger receptive field. This novel approach complements Micro Attention, augmenting the acquisition of multi-scale information.

3.3.2 Macro Attention. Drawing inspiration from the mechanism of dilated convolution, we incorporate it into the window division of attention in order to expand the receptive field. This adaptation effectively enhances the acquisition of global information while preserving linear complexity. Each window is inflated such that all windows fill the entire feature map without overlap. Macro Partition: $(G \times \frac{H}{G}, G \times \frac{W}{G}, C) \to (G^2, \frac{HW}{G^2}, C) \to (\frac{HW}{G^2}, G^2, C)$. After partition, we have the following formula.

$$\label{eq:MSA_Macro} \text{MSA}_{Macro}(\mathbf{Q}, \mathbf{K}, \mathbf{V}) = \left\{ \mathcal{A}_{Spatial}(\mathbf{Q}_j, \mathbf{K}_j, \mathbf{V}_j) \right\}_{j=0}^{\frac{HW}{G^2}}, \qquad (3)$$

where $\mathbf{Q}_j, \mathbf{K}_j, \mathbf{V}_j \in \mathbb{R}^{G^2 \times C}$ are dilated window queries, keys, and values. Each dilated window contains $\mathbf{G} \times \mathbf{G}$ patches.

3.4 Loss Function

We train our model with following loss function:

$$\mathcal{L}_{\text{Total}} = \lambda_1 \mathcal{L}_{\text{MAE}} + \lambda_2 \mathcal{L}_{\text{DEC}} + \lambda_3 \mathcal{L}_{\text{CR}}, \tag{4}$$

where \mathcal{L}_{MAE} denotes Mean absolute loss, \mathcal{L}_{DEC} the Pyramid decomposition loss and \mathcal{L}_{CR} the contrastive regularization.

3.4.1 Mean absolute loss. L_1 loss is used to characterize the error between the corrected image and the ground truth.

$$\mathcal{L}_{\text{MAE}} = \sum_{p=1}^{3HW} |Y(p) - T(p)|,$$
 (5)

where H, W are the height and width of the input size of the current image, respectively. T represents the ground truth and Y represents the network corrected image by bilateral interpolation to the original size image. p represents the pixels on the image.

3.4.2 Pyramid decomposition loss. This loss is used to measure the error between the decomposed corrected image and its ground truth layer by layer. These errors are proportionally merged together to form the loss of the decomposed image.

$$\mathcal{L}_{DEC} = \sum_{i=2}^{N} 2^{(i-2)} \sum_{p=1}^{3h_i w_i} |\mathbf{Y}_{(i)}(p) - \mathbf{T}_{(i)}(p)|, \tag{6}$$

where N represents the number of levels of the pyramid. $Y_{(i)}$ stands for i-th corrected pyramid output. $T_{(i)}$ represents the i-th gaussian pyramid layer decomposed from T. $h_i = \frac{1}{2^{i-1}}h$ and $w_i = \frac{1}{2^{i-1}}w$.

3.4.3 Contrastive regularization. As highlighted in existing contrast learning methods[5], diverse negative samples are vital for effective contrast learning. We propose a dynamic negative sample generation strategy, wherein for each input GT image, K negative samples are generated via gamma correction, with gamma values uniformly selected from the range [G1, G2]. Training with multiple negative samples enhances the model's generalizability to unseen exposure error images, crucial for improving performance and real-world applicability.

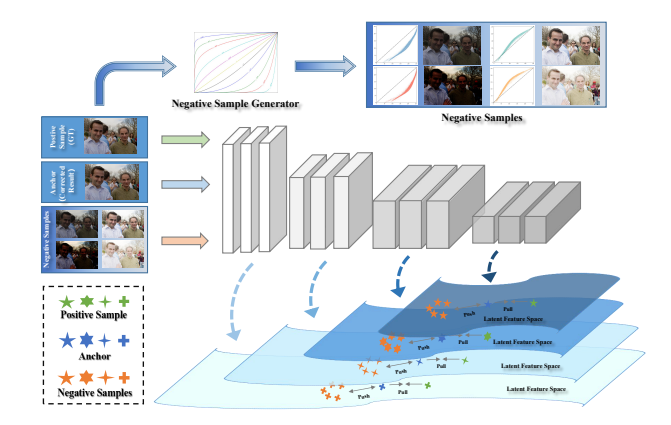


Figure 3: Adaptation Contrastive Regularization with Dynamic Negative Sample Generator

As shown in the Figure 3, we formulate a contrastive loss to minimize the distance between the correction result and the positive sample while maximizing the distance from the negative sample. A pre-trained network, R, is employed to extract features and apply contrastive regularization. The rich information obtained through feature extraction enables the contrastive loss to effectively contribute to the task.

$$\mathcal{L}_{CR} = \frac{\sum_{s=1}^{S} D(f_s, f_s^+)}{\sum_{k=1}^{K} \sum_{s=1}^{S} D(f_s, f_{ks}^-)},$$
 (7)

where $D(x, y) = ||x - y||_1$, $f_s = R(Y)$, $f_s^+ = R(T)$, $f_s^- = R(F)$, s = 1, 2, ..., S. K represents the number of samples generated by the negative sample generator. Both positive and negative samples are passed through the pre-trained VGG19 network, and the corrected image is downsampled S times. Y represents the corrected image, T represents the ground truth and F represents the negative images generated by Dynamic Negative Sample Generator.

4 EXPERIMENT

4.1 Implementation Details

We use the ADAM to optimize the network for 150 epochs with a initial learning rate of 1e-4. The weight of the loss function is set to $\lambda_1=1.0$, $\lambda_2=1.0$ and $\lambda_3=0.6$. The level of the Laplacian pyramid decomposition is N=4. The lowest gamma value is G1=0.3 and the highest gamma value is G2=2.8. The number of negative samples generated is K=6. The number of feature maps obtained by the feature extractor is S=4. Before training, we do data augmentation and resize the image to 512×512 ($h\times w$). We conduct all experiments with an NVIDIA 3090TI GPU.

4.2 Comparisons with State-of-the-Art Methods

We evaluate our proposed method by comparing it with existing SOTA methods. First, we examine quantitative metrics, employing the widely used peak signal-to-noise ratio (PSNR) and structural similarity (SSIM) as our evaluation indicators. To assess color performance, we utilize the Fréchet Inception Distance (FID)[16] to measure the similarity between two sets of images, the Colorfulness

Table 1: Quantitative comparisons on MSEC dataset. We compare each method with properly exposed reference image sets rendered by five expert photographers. The best results are highlighted with red. The second- and third-best results are highlighted in blue and green, respectively.

Method	Expe	rt A	Expe	rt B	Expert C		Expert D		Expert E		Avg	
Method	PSNR	SSIM	PSNR	SSIM	PSNR	SSIM	PSNR	SSIM	PSNR	SSIM	PSNR	SSIM
WVM[12]	14.488	0.788	15.803	0.699	15.117	0.678	15.863	0.693	16.469	0.704	15.548	0.688
LIME[14]	11.154	0.591	11.828	0.610	11.517	0.607	12.638	0.628	13.613	0.653	12.150	0.618
HDR CNN w/PS[10]	15.812	0.667	16.970	0.699	16.428	0.681	17.301	0.687	18.650	0.702	17.032	0.687
DPED (iPhone)[21]	15.134	0.609	16.505	0.636	15.907	0.622	16.571	0.627	17.251	0.649	16.274	0.629
DPED (BlackBerry)[21]	16.910	0.642	18.649	0.713	17.606	0.653	18.070	0.679	18.217	0.668	17.890	0.671
DPE (HDR)[6]	15.690	0.614	16.548	0.626	16.305	0.626	16.147	0.615	16.341	0.633	16.206	0.623
DPE (S-FiveK)[6]	16.933	0.678	17.701	0.668	17.741	0.696	17.572	0.674	17.601	0.670	17.510	0.677
RetinexNet[56]	10.759	0.585	11.613	0.596	11.135	0.605	11.987	0.615	12.671	0.636	11.633	0.607
Deep UPE[53]	13.161	0.610	13.901	0.642	13.689	0.632	14.806	0.649	15.678	0.667	14.247	0.640
Zero-DCE[13]	11.643	0.536	12.555	0.539	12.058	0.544	12.964	0.548	13.769	0.580	12.597	0.549
RUAS[40]	10.166	0.391	10.522	0.440	9.356	0.411	11.013	0.441	11.574	0.466	10.526	0.430
URetinex[59]	11.420	0.632	12.230	0.700	11.818	0.672	13.078	0.701	14.066	0.735	12.522	0.688
DALE[25]	13.294	0.691	14.324	0.757	13.734	0.722	14.256	0.743	14.511	0.763	14.024	0.735
IAT(local)[7]	16.610	0.750	17.520	0.822	16.950	0.780	17.020	0.780	16.430	0.789	16.910	0.783
MSEC[1]	19.158	0.746	20.096	0.734	20.205	0.769	18.975	0.719	18.983	0.727	19.483	0.739
IAT[7]	19.900	0.817	21.650	0.867	21.230	0.850	19.860	0.844	19.340	0.840	20.340	0.844
LCDPNet[52]	20.574	0.809	21.804	0.865	22.295	0.855	20.108	0.824	19.281	0.822	20.812	0.835
MMHT(Ours)	20.662	0.816	22.377	0.869	23.049	0.865	20.416	0.831	20.520	0.833	21.405	0.843

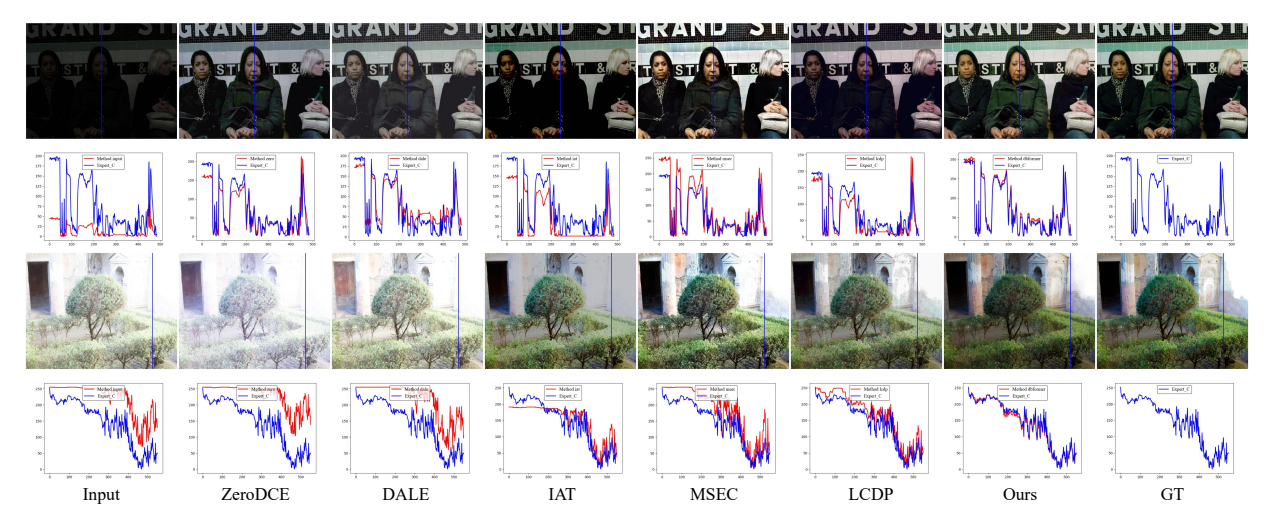


Figure 4: Qualitative comparisons on MSEC dataset. The blue line shows that the pixel values of the column are converted to perceived brightness and compared with that of ground truth.

Score (CF)[15] to gauge the richness of image colors, and additional metrics such as Δ CF and NIQE. Second, we conduct visual comparisons of exposure correction results to further substantiate the effectiveness of our method.

4.2.1 Quantitative Comparisons. The test set of MSEC contains 1181 sets of images of the same scene with five different exposures, accompanied by the correction results of five different experts. Table 1 shows that our method outperforms all existing methods in terms of PSNR and SSIM on all five expert test sets of MSEC. For color performance comparisons in Table 2, our method achieves the lowest FID, indicating that the proposed method is capable of producing realistic, natural and consistent images. In addition, the

lowest NIQE indicates that the corrected images of our method have the best subjective viewability. There are some methods that are closer to our method on CF, but the FIDs of these methods are much higher than ours, which means that they generate a lot of rare colors. Therefore, ΔCF is used to measure the difference between the CF of the corrected image and that of the expert image. A lower ΔCF indicates a more realistic color of the image. Our ΔCF is significantly better than all other methods. The performance comparisons are presented in the Figure 7 in the form of radar map. Each image of the LCDP dataset has both overexposed and underexposed areas. Our method also gains SOTA on LCDP dataset, which shows that the images corrected by our method are in excellent consistency.

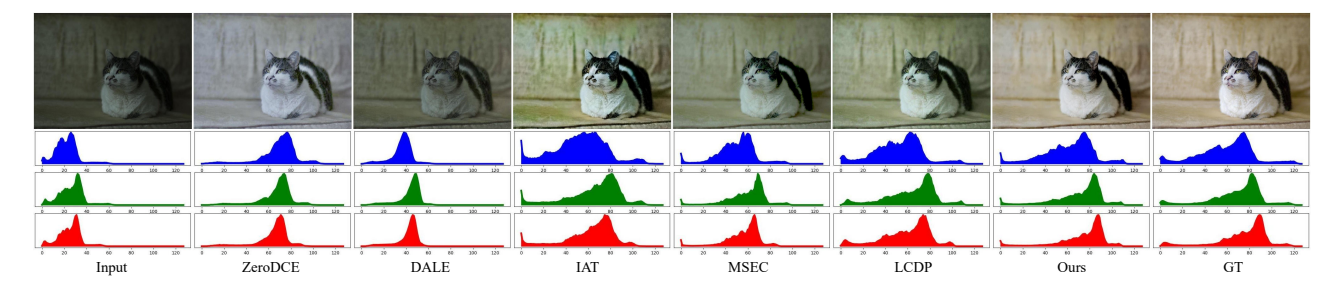


Figure 5: Compare the color performance of our method with other SOTA methods. Below the image is the RGB histogram.



Figure 6: The consistency of correction results between our method and existing methods is compared. The correction results of overexposure and underexposure are concatenated.

Table 2: Quantitative comparisons of color performance on MSEC and LCDP datasets.

Methods(MSEC)	PNSR↑	SSIM↑	FID↓	CF↑	Δ CF↓	NIQE↓
RUAS	9.356	0.411	30.125	22.612	19.792	4.643
URetinex	11.818	0.672	27.451	28.597	13.807	2.654
MSEC	20.205	0.769	20.264	38.898	3.506	2.838
IAT	21.230	0.850	12.091	37.188	5.216	3.132
LCDP	22.295	0.855	12.752	33.293	9.111	2.914
(MMHT)Ours	23.049	0.865	10.223	40.202	2.202	2.339
Methods(LCDP)	PNSR↑	SSIM↑	FID	CF↑	Δ CF.I.	NIOEL
						11122
LIME	17.335	0.686	47.725	32.949	6.077	4.248
LIME IAT	17.335 18.842	0.686 0.684	47.725 37.516	32.949 32.143		~ •
	-,				6.077	4.248
IAT	18.842	0.684	37.516	32.143	6.077 6.883	4.248 2.975
IAT RetinexNet	18.842 19.250	0.684 0.704	37.516 52.723	32.143 33.541	6.077 6.883 5.485	4.248 2.975 4.947

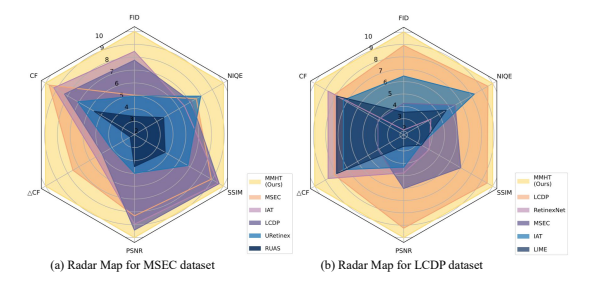


Figure 7: Radar Map for Performance Comparisons.

4.2.2 Qualitative Comparisons. Figure 4 presents a comparison of image quality between our method and SOTA methods. For both underexposed and overexposed images, our method accurately corrects them to the proper exposure state. In Figure 6, we evaluate the consistency of correction results by comparing corrected images

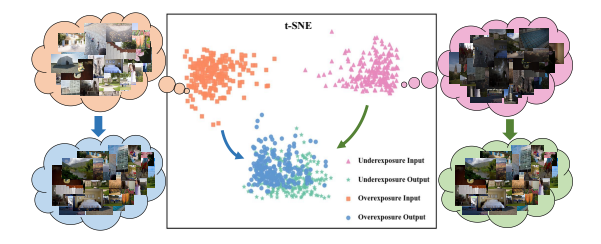


Figure 8: t-SNE visualization to show correction consistency.

produced by our method with those corrected by existing methods. Our method's results exhibit remarkable consistency, displaying not only similar color and brightness but also eliminating differences in outcomes due to input variations. Furthermore, as illustrated in Figure 5, images corrected by our method boast both the most visually appealing color performance and superior detail preservation. In contrast, other methods either introduce inconsistent lighting or generate color distortion. Furthermore, as can be seen in Figure 8, after being processed by MMHT, the underexposure and overexposure representations tend to be intersected together.

4.3 Image Enhancement Results

For LOL dataset[56], the compared methods include Zero-DCE[13], RetiNexNet[56], MBLLEN[42], DRBN[60], KIND++[68], RCT[24], IAT[7]. For MIT-Adobe FiveK dataset[2], the compared methods include White-Box[17], U-Net[49], DPE[6], DPED[21], D-UPE[53], D-LPF[46], STAR[70], IAT[7]. The quantitative comparisons with existing methods are shown in Figure 11, which proves that our method also performs superior in low light scenes.



Figure 9: Detection results on DarkFace dataset.

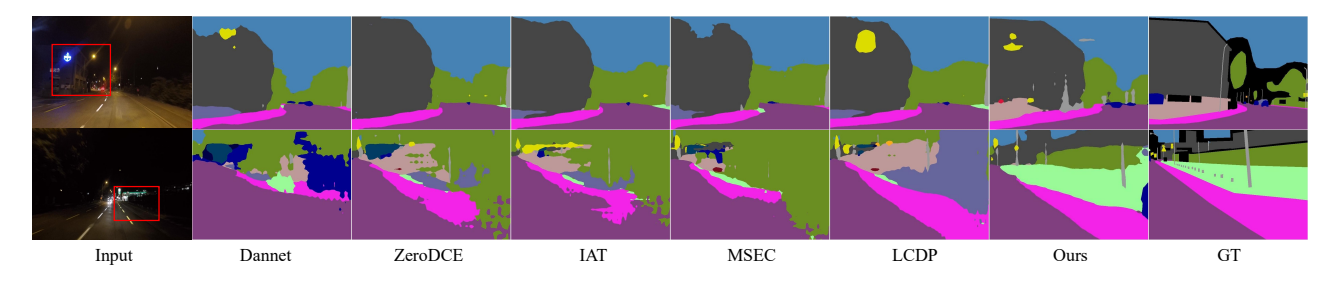


Figure 10: Segmentation results on ACDC-Nighttime dataset.

Table 3: Performance comparisons on high-level tasks. We retrain the detector/segmentator in all cases containing the enhancer.

Task	D	ark Face De	tector	Enhancer + Detector (Finetune)							
Method	HLA[54]	REG[29]	MEAT[8]	LIME[14]	ZeroDCE[13]	MSEC[1]	RUAS[40]	LCDP[52]	IAT[7]	MMHT(Ours)	
mAP	0.607	0.514	0.526	0.644	0.665	0.659	0.642	0.654	0.663	0.675	
Task	Nighttime Semantic Segmentator			Enhancer + Segmentator (Finetune)							
Method	DANNet[59]	CIC[27]	GPS-GLASS[26]	LIME[14]	ZeroDCE[13]	MSEC[1]	RUAS[40]	LCDP[52]	IAT[7]	MMHT(Ours)	
mIoU	0.398	0.264	0.380	0.447	0.452	0.449	0.448	0.455	0.456	0.461	

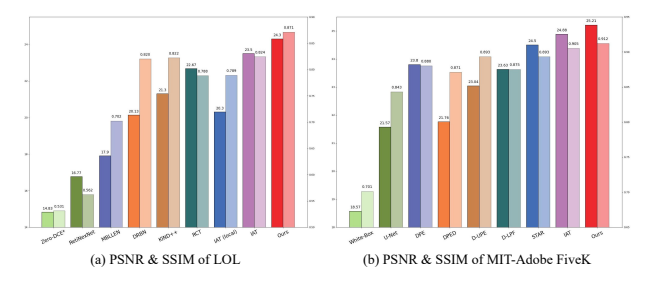


Figure 11: Quantitative comparisons on LOL and MIT-5K.

4.4 High-level Vision Applications

To demonstrate the generalizability of our method, we apply it to relevant high level vision tasks, including low-light face and low-light semantic segmentation tasks.

Here we adopt the DARKFACE[61] and ACDC[50] datasets for evaluating low-light detection and segmentation respectively. To fully evaluate its performance, we not only compare some of the correction methods, but also consider specific detection methods and segmentation methods. The quantitative comparisons with existing methods are shown in Figure 9 and 10 while quantitative results are in the Table 3. Both quantitatively and quantitatively demonstrate the significance of our method for downstream tasks.

4.5 Ablation Study

4.5.1 Experiment on Transformer and Convolution Arrangement and the Effect of Laplacian Pyramid Decomposition. To explore the optimal arrangement of transformer and convolution, we design an ablation study for the network used in each stage, with results in Table 4. As U-Net is progressively replaced by the MMT Restorer, the quantitative results improve. However, there is a slight drop in PSNR and SSIM when the last network is replaced, as removing the convolution entirely eliminates the inductive bias. Combining convolution with transformers yields the better results, with R1, R2, R3 as the best pipeline. We also conduct ablation experiments on Laplacian pyramid decomposition. As shown in the Table 4 and Figure 12(a), MMT Restorer performs well even without Laplacian pyramid decomposition but compromises the coarse-to-fine correction, negatively impacting results qualitatively and quantitatively.

4.5.2 Experiments on the Effect of Macro-Micro Attention. Global information acquisition is crucial for addressing image exposure correction issues. However, the micro attention restricts operations to a single window and loses long-range dependencies. We introduce macro attention with a larger receptive field in combination with micro attention to effectively acquire multi-scale information. An ablation study is designed for macro-micro attention, with results presented in Table 5. Replacing either micro or macro attention

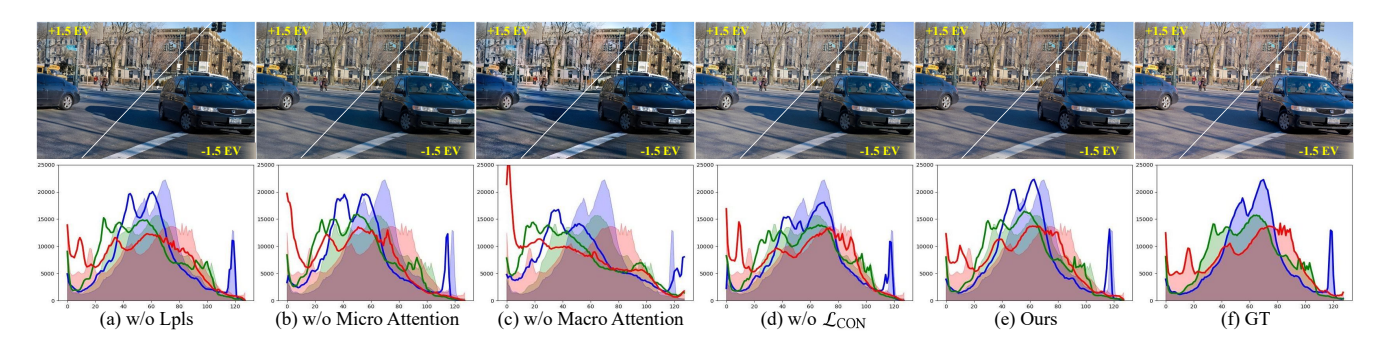


Figure 12: Visualization results of ablation experiments are shown. The GT images are filled RGB curves while the ablation experimental images are unfilled RGB curves.

Table 4: Exploring Transformer and Convolution Arrangement and the effect of Laplacian Pyramid Decomposition. R1 means replacing the U-Net Restorer with MMT Restorer in stage 1 of the pipeline.

R1	R2	R3	R4	Lpls	PSNR↑	SSIM↑	Δ CF↓	FID↓
-	-	-	-	Х	22.785	0.853	2.119	10.331
X	Х	Х	Х	/	20.517	0.771	3.419	20.964
1	X	X	Х	/	21.875	0.811	3.331	15.397
1	1	X	Х	/	22.269	0.831	2.798	13.778
1	1	1	Х	/	23.049	0.865	2.202	10.223
1	✓	✓	✓	1	22.971	0.859	2.229	10.414

with the other results in a significant increase in FID and CF with a decrease in PSNR and SSIM. Furthermore, swapping their order also inflicts a slight detriment to these metrics. In the Figure 12(c), we observe that omitting macro attention severely impacts the results, causing substantial color distortions and artifacts.

4.5.3 Experiment on the Effect of Contrastive Regularization. To examine the effect of contrastive loss, we remove the contrastive loss in the adjusting attention order. As shown in the Table 5, there is a significant reduction in the PSNR and SSIM. Figure 12(d) shows that removing contrastive learning leads to inconsistent correction results for different exposure inputs. Contrastive constraint encourages the model to learn features distinguishing well-exposed images from exposure-error images. Using abundant negative samples forces the model to learn more discriminative features, resulting in consistent exposure correction performance.

Table 5: Exploring the effect of Macro-Micro Attention and Contrastive Regularization.

Mic	Mac	Mic-Mac	Mac-Mic	L_{CR}	PSNR↑	SSIM↑	Δ CF↓	FID↓
/	Х	Х	Х	Х	22.092	0.823	3.945	16.712
Х	1	X	Х	X	22.325	0.836	2.616	12.301
X	Х	1	X	Х	22.791	0.843	2.419	11.818
X	X	X	✓	X	22.901	0.851	2.305	10.597
_/	Х	Х	Х	/	22.225	0.835	3.978	16.645
Х	1	X	Х	1	22.494	0.846	2.511	12.219
X	Х	1	X	/	22.949	0.862	2.415	11.774
X	X	X	/	1	23.049	0.865	2.202	10.223

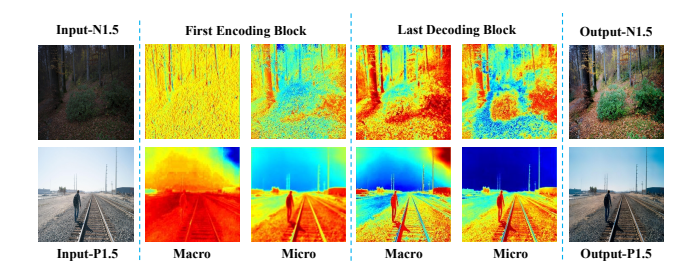


Figure 13: Visualization of heat maps from the first encoding block and last decoding block.

4.6 Feature map visualization

To further explain the role of multiple attention and hierarchical network structure, we visualize the feature map after processing of the first block of the encoder in stage 1 and the last block of the decoder in stage 3. The results are presented in the Figure 13. Longrange dependencies appear after macro attention, while short-range dependencies appear after micro attention. This aids the network in adapting different adjustments based on varying semantics.

5 CONCLUSION

In this paper, we address the issues of inconsistent results and color distortion in exposure correction tasks. To model long-range dependencies, a Macro-Micro attention mechanism has been developed, which significantly enhances image color and detail. A contrastive constraint is then established to effectively resolve inconsistent correction results. By integrating the advantages of both transformer and convolution, a four-stage pipeline is constructed, which further improves the quality of corrected images. Our proposed model is assessed on multiple challenging exposure-error datasets and applied as an enhancer for high-level tasks. Results demonstrate that our approach significantly outperforms state-of-the-art methods, indicating its potential applicability in exposure-related tasks.

ACKNOWLEDGMENTS

This work is partially supported by the National Key R&D Program of China (No. 2022YFA1004101), the National Natural Science Foundation of China (No. U22B2052).

REFERENCES

- Mahmoud Afifi, Konstantinos G Derpanis, Bjorn Ommer, and Michael S Brown.
 Learning multi-scale photo exposure correction. In Proceedings of the IEEE/CVF Conference on Computer Vision and Pattern Recognition. 9157–9167.
- [2] Vladimir Bychkovsky, Sylvain Paris, Eric Chan, and Frédo Durand. 2011. Learning photographic global tonal adjustment with a database of input/output image pairs. In CVPR 2011. IEEE, 97–104.
- [3] Bolun Cai, Xianming Xu, Kailing Guo, Kui Jia, Bin Hu, and Dacheng Tao. 2017. A joint intrinsic-extrinsic prior model for retinex. In Proceedings of the IEEE international conference on computer vision. 4000–4009.
- [4] Jiawen Chen, Andrew Adams, Neal Wadhwa, and Samuel W Hasinoff. 2016. Bilateral guided upsampling. ACM Transactions on Graphics (TOG) 35, 6 (2016), 1–8.
- [5] Ting Chen, Simon Kornblith, Mohammad Norouzi, and Geoffrey Hinton. 2020. A simple framework for contrastive learning of visual representations. In *Interna*tional conference on machine learning. PMLR, 1597–1607.
- [6] Yu-Sheng Chen, Yu-Ching Wang, Man-Hsin Kao, and Yung-Yu Chuang. 2018. Deep photo enhancer: Unpaired learning for image enhancement from photographs with gans. In Proceedings of the IEEE Conference on Computer Vision and Pattern Recognition. 6306–6314.
- [7] Ziteng Cui, Kunchang Li, Lin Gu, Shenghan Su, Peng Gao, Zhengkai Jiang, Yu Qiao, and Tatsuya Harada. 2022. Illumination Adaptive Transformer. arXiv preprint arXiv:2205.14871 (2022).
- [8] Ziteng Cui, Guo-Jun Qi, Lin Gu, Shaodi You, Zenghui Zhang, and Tatsuya Harada. 2021. Multitask aet with orthogonal tangent regularity for dark object detection. In Proceedings of the IEEE/CVF International Conference on Computer Vision. 2553–2562.
- [9] Zihang Dai, Hanxiao Liu, Quoc V Le, and Mingxing Tan. 2021. Coatnet: Marrying convolution and attention for all data sizes. Advances in Neural Information Processing Systems 34 (2021), 3965–3977.
- [10] Gabriel Eilertsen, Joel Kronander, Gyorgy Denes, Rafał K Mantiuk, and Jonas Unger. 2017. HDR image reconstruction from a single exposure using deep CNNs. ACM transactions on graphics (TOG) 36, 6 (2017), 1–15.
- [11] F Eyiokur, Dogucan Yaman, Hazim Kemal Ekenel, and Alexander Waibel. 2022. Exposure Correction Model to Enhance Image Quality. In Proceedings of the IEEE/CVF Conference on Computer Vision and Pattern Recognition. 676–686.
- [12] Xueyang Fu, Delu Zeng, Yue Huang, Xiao-Ping Zhang, and Xinghao Ding. 2016. A weighted variational model for simultaneous reflectance and illumination estimation. In Proceedings of the IEEE conference on computer vision and pattern recognition. 2782–2790.
- [13] Chunle Guo, Chongyi Li, Jichang Guo, Chen Change Loy, Junhui Hou, Sam Kwong, and Runmin Cong. 2020. Zero-reference deep curve estimation for lowlight image enhancement. In Proceedings of the IEEE/CVF Conference on Computer Vision and Pattern Recognition. 1780–1789.
- [14] Xiaojie Guo. 2016. LIME: A method for low-light image enhancement. In Proceedings of the 24th ACM international conference on Multimedia. 87–91.
- [15] David Hasler and Sabine E Suesstrunk. 2003. Measuring colorfulness in natural images. In Human vision and electronic imaging VIII, Vol. 5007. SPIE, 87–95.
- [16] Martin Heusel, Hubert Ramsauer, Thomas Unterthiner, Bernhard Nessler, and Sepp Hochreiter. 2017. Gans trained by a two time-scale update rule converge to a local nash equilibrium. Advances in neural information processing systems 30 (2017).
- [17] Yuanming Hu, Hao He, Chenxi Xu, Baoyuan Wang, and Stephen Lin. 2018. Exposure: A white-box photo post-processing framework. ACM Transactions on Graphics (TOG) 37, 2 (2018), 1–17.
- [18] Jie Huang, Yajing Liu, Xueyang Fu, Man Zhou, Yang Wang, Feng Zhao, and Zhiwei Xiong. 2022. Exposure Normalization and Compensation for Multiple-Exposure Correction. In Proceedings of the IEEE/CVF Conference on Computer Vision and Pattern Recognition (CVPR). 6043–6052.
- [19] Jie Huang, Feng Zhao, Man Zhou, Jie Xiao, Naishan Zheng, Kaiwen Zheng, and Zhiwei Xiong. 2023. Learning Sample Relationship for Exposure Correction. In Proceedings of the IEEE/CVF Conference on Computer Vision and Pattern Recognition (CVPR). 9904–9913.
- [20] Jie Huang, Man Zhou, Yajing Liu, Mingde Yao, Feng Zhao, and Zhiwei Xiong. 2022. Exposure-Consistency Representation Learning for Exposure Correction. In Proceedings of the 30th ACM International Conference on Multimedia. 6309–6317.
- [21] Andrey Ignatov, Nikolay Kobyshev, Radu Timofte, Kenneth Vanhoey, and Luc Van Gool. 2017. Dslr-quality photos on mobile devices with deep convolutional networks. In Proceedings of the IEEE International Conference on Computer Vision. 3277–3285.
- [22] Zhiying Jiang, Zhuoxiao Li, Shuzhou Yang, Xin Fan, and Risheng Liu. 2022. Target oriented perceptual adversarial fusion network for underwater image enhancement. IEEE Transactions on Circuits and Systems for Video Technology 32, 10 (2022), 6584–6598.
- [23] Feng Zhao Keyu Yan Jinghao Zhang Yukun Huang Man Zhou Zhiwei Xiong Jie Huang, Yajing Liu. 2022. Deep Fourier-based Exposure Correction Network with Spatial-Frequency Interaction. In Proceedings of the European Conference on

- Computer Vision (ECCV).
- [24] Hanul Kim, Su-Min Choi, Chang-Su Kim, and Yeong Jun Koh. 2021. Representative color transform for image enhancement. In Proceedings of the IEEE/CVF International Conference on Computer Vision. 4459–4468.
- [25] Dokyeong Kwon, Guisik Kim, and Junseok Kwon. 2020. DALE: Dark region-aware low-light image enhancement. arXiv preprint arXiv:2008.12493 (2020).
- [26] Hongjae Lee, Changwoo Han, and Seung-Won Jung. 2022. GPS-GLASS: Learning Nighttime Semantic Segmentation Using Daytime Video and GPS data. arXiv preprint arXiv:2207.13297 (2022).
- [27] Attila Lengyel, Sourav Garg, Michael Milford, and Jan C van Gemert. 2021. Zeroshot day-night domain adaptation with a physics prior. In Proceedings of the IEEE/CVF International Conference on Computer Vision. 4399–4409.
- [28] Jiawei Li, Jinyuan Liu, Shihua Zhou, Qiang Zhang, and Nikola K Kasabov. 2022. Learning a coordinated network for detail-refinement multiexposure image fusion. IEEE Transactions on Circuits and Systems for Video Technology 33, 2 (2022), 713–727
- [29] Jinxiu Liang, Jingwen Wang, Yuhui Quan, Tianyi Chen, Jiaying Liu, Haibin Ling, and Yong Xu. 2021. Recurrent exposure generation for low-light face detection. IEEE Transactions on Multimedia 24 (2021), 1609–1621.
- [30] Jinyuan Liu, Xin Fan, Zhanbo Huang, Guanyao Wu, Risheng Liu, Wei Zhong, and Zhongxuan Luo. 2022. Target-aware dual adversarial learning and a multi-scenario multi-modality benchmark to fuse infrared and visible for object detection. In Proceedings of the IEEE/CVF Conference on Computer Vision and Pattern Recognition. 5802–5811.
- [31] Jinyuan Liu, Xin Fan, Ji Jiang, Risheng Liu, and Zhongxuan Luo. 2021. Learning a deep multi-scale feature ensemble and an edge-attention guidance for image fusion. *IEEE Transactions on Circuits and Systems for Video Technology* 32, 1 (2021), 105–119.
- [32] Jinyuan Liu, Jingjie Shang, Risheng Liu, and Xin Fan. 2022. Attention-guided global-local adversarial learning for detail-preserving multi-exposure image fusion. IEEE Transactions on Circuits and Systems for Video Technology 32, 8 (2022), 5026–5040.
- [33] Jinyuan Liu, Guanyao Wu, Junsheng Luan, Zhiying Jiang, Risheng Liu, and Xin Fan. 2023. HoLoCo: Holistic and local contrastive learning network for multi-exposure image fusion. *Information Fusion* 95 (2023), 237–249.
- [34] Jinyuan Liu, Yuhui Wu, Zhanbo Huang, Risheng Liu, and Xin Fan. 2021. Smoa: Searching a modality-oriented architecture for infrared and visible image fusion. IEEE Signal Processing Letters 28 (2021), 1818–1822.
- [35] Risheng Liu, Xin Fan, Ming Zhu, Minjun Hou, and Zhongxuan Luo. 2020. Real-world underwater enhancement: Challenges, benchmarks, and solutions under natural light. IEEE transactions on circuits and systems for video technology 30, 12 (2020), 4861–4875.
- [36] Risheng Liu, Zhiying Jiang, Shuzhou Yang, and Xin Fan. 2022. Twin adversarial contrastive learning for underwater image enhancement and beyond. IEEE Transactions on Image Processing 31 (2022), 4922–4936.
- [37] Risheng Liu, Zhouchen Lin, Fernando De la Torre, and Zhixun Su. 2012. Fixed-rank representation for unsupervised visual learning. In 2012 ieee conference on computer vision and pattern recognition. IEEE, 598–605.
- [38] Risheng Liu, Jinyuan Liu, Zhiying Jiang, Xin Fan, and Zhongxuan Luo. 2020. A bilevel integrated model with data-driven layer ensemble for multi-modality image fusion. *IEEE Transactions on Image Processing* 30 (2020), 1261–1274.
- [39] Risheng Liu, Long Ma, Tengyu Ma, Xin Fan, and Zhongxuan Luo. 2022. Learning with nested scene modeling and cooperative architecture search for low-light vision. IEEE Transactions on Pattern Analysis and Machine Intelligence 45, 5 (2022), 5953–5969.
- [40] Risheng Liu, Long Ma, Jiaao Zhang, Xin Fan, and Zhongxuan Luo. 2021. Retinexinspired unrolling with cooperative prior architecture search for low-light image enhancement. In Proceedings of the IEEE/CVF Conference on Computer Vision and Pattern Recognition. 10561–10570.
- [41] Ze Liu, Yutong Lin, Yue Cao, Han Hu, Yixuan Wei, Zheng Zhang, Stephen Lin, and Baining Guo. 2021. Swin transformer: Hierarchical vision transformer using shifted windows. In Proceedings of the IEEE/CVF International Conference on Computer Vision. 10012–10022.
- [42] Feifan Lv, Feng Lu, Jianhua Wu, and Chongsoon Lim. 2018. MBLLEN: Low-Light Image/Video Enhancement Using CNNs.. In BMVC, Vol. 220. 4.
- [43] Long Ma, Dian Jin, Nan An, Jinyuan Liu, Xin Fan, and Risheng Liu. 2023. Bilevel Fast Scene Adaptation for Low-Light Image Enhancement. arXiv preprint arXiv:2306.01343 (2023).
- [44] Long Ma, Risheng Liu, Yiyang Wang, Xin Fan, and Zhongxuan Luo. 2022. Low-light image enhancement via self-reinforced retinex projection model. IEEE Transactions on Multimedia (2022).
- [45] Long Ma, Tianjiao Ma, Xinwei Xue, Xin Fan, Zhongxuan Luo, and Risheng Liu. 2022. Practical Exposure Correction: Great Truths Are Always Simple. arXiv preprint arXiv:2212.14245 (2022).
- [46] Sean Moran, Pierre Marza, Steven McDonagh, Sarah Parisot, and Gregory Slabaugh. 2020. Deeplpf: Deep local parametric filters for image enhancement. In Proceedings of the IEEE/CVF conference on computer vision and pattern recognition. 12826–12835.

- [47] Yongri Piao, Wei Ji, Jingjing Li, Miao Zhang, and Huchuan Lu. 2019. Depthinduced multi-scale recurrent attention network for saliency detection. In Proceedings of the IEEE/CVF international conference on computer vision. 7254–7263.
- [48] Yongri Piao, Zhengkun Rong, Miao Zhang, Weisong Ren, and Huchuan Lu. 2020. A2dele: Adaptive and attentive depth distiller for efficient RGB-D salient object detection. In Proceedings of the IEEE/CVF conference on computer vision and pattern recognition. 9060–9069.
- [49] Olaf Ronneberger, Philipp Fischer, and Thomas Brox. 2015. U-net: Convolutional networks for biomedical image segmentation. In *International Conference on Medical image computing and computer-assisted intervention*. Springer, 234–241.
- [50] Christos Sakaridis, Dengxin Dai, and Luc Van Gool. 2021. ACDC: The adverse conditions dataset with correspondences for semantic driving scene understanding. In Proceedings of the IEEE/CVF International Conference on Computer Vision. 10765–10775.
- [51] Wenzhe Shi, Jose Caballero, Ferenc Huszár, Johannes Totz, Andrew P Aitken, Rob Bishop, Daniel Rueckert, and Zehan Wang. 2016. Real-time single image and video super-resolution using an efficient sub-pixel convolutional neural network. In Proceedings of the IEEE conference on computer vision and pattern recognition. 1874–1883
- [52] Haoyuan Wang, Ke Xu, and Rynson WH Lau. 2022. Local color distributions prior for image enhancement. In European Conference on Computer Vision. Springer, 343–359.
- [53] Ruixing Wang, Qing Zhang, Chi-Wing Fu, Xiaoyong Shen, Wei-Shi Zheng, and Jiaya Jia. 2019. Underexposed photo enhancement using deep illumination estimation. In Proceedings of the IEEE/CVF Conference on Computer Vision and Pattern Recognition. 6849–6857.
- [54] Wenjing Wang, Xinhao Wang, Wenhan Yang, and Jiaying Liu. 2022. Unsupervised face detection in the dark. IEEE Transactions on Pattern Analysis and Machine Intelligence 45, 1 (2022), 1250–1266.
- [55] Zhendong Wang, Xiaodong Cun, Jianmin Bao, Wengang Zhou, Jianzhuang Liu, and Houqiang Li. 2022. Uformer: A general u-shaped transformer for image restoration. In Proceedings of the IEEE/CVF Conference on Computer Vision and Pattern Recognition. 17683–17693.
- [56] Chen Wei, Wenjing Wang, Wenhan Yang, and Jiaying Liu. 2018. Deep retinex decomposition for low-light enhancement. arXiv preprint arXiv:1808.04560 (2018).
- [57] Haiping Wu, Bin Xiao, Noel Codella, Mengchen Liu, Xiyang Dai, Lu Yuan, and Lei Zhang. 2021. Cvt: Introducing convolutions to vision transformers. In Proceedings of the IEEE/CVF International Conference on Computer Vision. 22–31.
- [58] Jianlong Wu, Zhouchen Lin, and Hongbin Zha. 2019. Essential tensor learning for multi-view spectral clustering. *IEEE Transactions on Image Processing* 28, 12 (2019), 5910–5922.
- [59] Jun Xu, Yingkun Hou, Dongwei Ren, Li Liu, Fan Zhu, Mengyang Yu, Haoqian Wang, and Ling Shao. 2020. Star: A structure and texture aware retinex model.

- IEEE Transactions on Image Processing 29 (2020), 5022-5037.
- [60] Wenhan Yang, Shiqi Wang, Yuming Fang, Yue Wang, and Jiaying Liu. 2020. From fidelity to perceptual quality: A semi-supervised approach for low-light image enhancement. In Proceedings of the IEEE/CVF conference on computer vision and pattern recognition. 3063–3072.
- [61] Wenhan Yang, Ye Yuan, Wenqi Ren, Jiaying Liu, Walter J Scheirer, Zhangyang Wang, Taiheng Zhang, Qiaoyong Zhong, Di Xie, Shiliang Pu, et al. 2020. Advancing image understanding in poor visibility environments: A collective benchmark study. IEEE Transactions on Image Processing 29 (2020), 5737–5752.
- [62] Kun Yuan, Shaopeng Guo, Ziwei Liu, Aojun Zhou, Fengwei Yu, and Wei Wu. 2021. Incorporating convolution designs into visual transformers. In Proceedings of the IEEE/CVF International Conference on Computer Vision. 579–588.
- [63] Syed Waqas Zamir, Aditya Arora, Salman Khan, Munawar Hayat, Fahad Shah-baz Khan, and Ming-Hsuan Yang. 2022. Restormer: Efficient transformer for high-resolution image restoration. In Proceedings of the IEEE/CVF Conference on Computer Vision and Pattern Recognition. 5728–5739.
- [64] Haokui Zhang, Wenze Hu, and Xiaoyu Wang. 2022. EdgeFormer: Improving Light-weight ConvNets by Learning from Vision Transformers. arXiv preprint arXiv:2203.03952 (2022).
- [65] Jinghao Zhang, Jie Huang, Mingde Yao, Man Zhou, and Feng Zhao. 2022. Structure- and Texture-Aware Learning for Low-Light Image Enhancement. In Proceedings of the 30th ACM International Conference on Multimedia. 6483–6492.
- [66] Miao Zhang, Weisong Ren, Yongri Piao, Zhengkun Rong, and Huchuan Lu. 2020. Select, supplement and focus for RGB-D saliency detection. In Proceedings of the IEEE/CVF conference on computer vision and pattern recognition. 3472–3481.
- [67] Qing Zhang, Ganzhao Yuan, Chunxia Xiao, Lei Zhu, and Wei-Shi Zheng. 2018. High-quality exposure correction of underexposed photos. In Proceedings of the 26th ACM international conference on Multimedia. 582–590.
- [68] Yonghua Zhang, Xiaojie Guo, Jiayi Ma, Wei Liu, and Jiawan Zhang. 2021. Beyond brightening low-light images. International Journal of Computer Vision 129 (2021), 1013–1037
- [69] Yonghua Zhang, Jiawan Zhang, and Xiaojie Guo. 2019. Kindling the darkness: A practical low-light image enhancer. In Proceedings of the 27th ACM international conference on multimedia. 1632–1640.
- [70] Zhaoyang Zhang, Yitong Jiang, Jun Jiang, Xiaogang Wang, Ping Luo, and Jinwei Gu. 2021. Star: A structure-aware lightweight transformer for real-time image enhancement. In Proceedings of the IEEE/CVF International Conference on Computer Vision. 4106–4115.
- [71] Naishan Zheng, Jie Huang, Feng Zhao, Xueyang Fu, and Feng Wu. 2022. Unsupervised Underexposed Image Enhancement via Self-Illuminated and Perceptual Guidance. *IEEE Transactions on Multimedia* (2022), 1–16. https://doi.org/10.1109/TMM.2022.3193059